A Novel Ratiometric Fluorescent Approach for the Modulation of the Dynamic Range of Lateral Flow Immunoassays

Amadeo Sena-Torralba, Helena Torné-Morató, Claudio Parolo,* Saba Ranjbar, Mohammad Amin Farahmand Nejad, Ruslan Álvarez-Diduk, Andrea Idili, Mohammad Reza Hormozi-Nezhad, and Arben Merkoçi*

The majority of lateral flow assays (LFAs) use single-color optical labels to provide a qualitative naked-eye detection, however this detection method displays two important limitations. First, the use of a single-color label makes the LFA prone to results misinterpretation. Second, it does not allow the precise modulation of the sensitivity and dynamic range of the test. To overcome these limitations, a ratiometric approach is developed. In particular, using anti-HIgG functionalized red-fluorescent quantum dots on the conjugate pad (as target dependent labels) and blue-fluorescent nanoparticles fixed on the test line (as target independent reporters), it is possible to generate a wide color palette (blue, purple, pink, red) on the test line. It is believed that this strategy will facilitate the development of LFAs by easily adjusting their analytical properties to the needs required by the specific application.

A. Sena-Torralba, H. Torné-Morató, C. Parolo, S. Ranjbar,
M. A. Farahmand Nejad, R. Álvarez-Diduk, A. Idili, A. Merkoçi
Nanobioelectronics & Biosensors Group
Institut Català de Nanociència i Nanotecnologia (ICN2)
CSIC and The Barcelona Institute of Science and Technology (BIST)
Campus UAB, Bellaterra, Barcelona 08193, Spain
E-mail: claudio.parolo@isglobal.org; arben.merkoci@icn2.cat
M. A. Farahmand Nejad, M. R. Hormozi-Nezhad
Department of Chemistry
Sharif University of Technology
Tehran 11155-9516, Iran
M. R. Hormozi-Nezhad
Institute for Nanoscience and Nanotechnology
Sharif University of Technology
Tehran 11155-9516, Iran
A. Merkoçi
Catalan Institution for Research and Advanced Studies (ICREA)
Pg. Lluís Companys 23, Barcelona 08010, Spain

1. Introduction

During the last few decades, lateral flow assays (LFA) have proven to be one of the most successful point-of-care diagnostic tests, both in clinical and environmental applications.[1–4] Paper-based biosensors offer several important advantages such as cost-effectiveness, sustainability, washing-free operability, and high tunability.[5,6] Additionally, thanks to their ease of use, speed, and simplicity, LFAs are routinely used for applications requiring mass-testing and qualitative evaluation.[2,7,8] For example, LFAs are commonly used to diagnose pregnancy at home[9] or, more recently, to quickly identify the presence of COVID-19-specific antibodies and antigens in pharmacies and mobile testing sites.[7,10,11] Despite this, their recognized low sensitivity[12] and difficulty to interpret faint bands[13] are still hampering their use in challenging clinical applications, where a quantitative detection of the target analyte is required.[14] To overcome this limitation, researchers have developed different strategies able to enhance the sensitivity in LFA[12,15–18] and to allow on-site assay quantification.[19–21] However, these approaches are still mostly confined to academic laboratories, due to their complexity and potentially high cost that would affect the affordability and usability of LFAs in real settings.[22] Therefore, there is an urgent need for simple and cost-effective strategies that can overcome the aforementioned limitations of LFA allowing their implementation in a wide range of clinical scenarios.

Currently, the majority of LFAs exploit colorimetric labels (e.g., gold nanoparticles and polystyrene beads)[23,24] that allow for a convenient naked-eye or smartphone-based detection. The former is still the preferred detection mode of LFAs, since it is equipment-free and cost-effective, therefore, ideal for resource-limited settings.[25] Instead, the latter method is on the rise (thanks to the ubiquity of smartphones) and tends to improve test reproducibility (i.e., removing the subjective part of the naked-eye detection).[26–30] In both cases, however, the use of a colorimetric label limits the readout of an LFA to the identification/measurement of a single-color signal. Unfortunately, this may generate uncertain situations when the presence of faint bands may not

**ADVANCED
SCIENCE NEWS**

www.advancedsciencenews.com

**ADVANCED
MATERIALS
TECHNOLOGIES**

www.advmattechnol.de

be obvious to the final, untrained user[31] or difficult to detect even with the smartphone under sub-optimal light conditions.[32] Additionally, LFAs based on the generation of a single-color signal display a poorly tunable dynamic range (the minimum to maximum range of concentrations that can be detected), which can affect the adaptation of the LFA to different applications requiring the detection of the same biomarker, but at different concentrations. In this sense, time consuming sample pre-treatment (concentration or dilution) must be performed in order to drop the target's concentration in the quantitative range.[33]

During the millennia the human eye has evolved to distinguish different color tonalities rather than different color intensities.[34] For example, we had to distinguish between potentially poisonous red mushrooms from nutritious brown ones.[35,36] In this work, we demonstrate how harnessing this concept it is possible to create more sensitive and precise LFAs able to support naked-eye detection. We achieved it using a ratiometric approach, which consists in mixing two fluorescent labels to generate a wide color variation.[37] Ratiometric readouts are not new in the bioanalytical field, since they have been used for applications ranging from pH sensing[38] to the detection of several molecular targets (e.g., thrombin,[39] botulinum neurotoxin,[40] and bovine hemoglobin[41]). In the field of paper-based sensors, ratiometric approaches have been employed for the detection of diverse analytes, ranging from heavy metal ions[42] to protein biomarkers[43] (see Table S1, Supporting Information for previous studies). In all these cases, ratiometry has been applied either as a sensitivity enhancement strategy[44–46] or as a tool to reduce background interfering signals.[47]

Here, we propose for the first time the implementation of a ratiometric approach in a paper-based sensor for the precise modulation of a LFA's dynamic range using human IgG (H-IgG) as a model analyte. Specifically, we demonstrate how we can easily modify the color tonality in the LFA's detection line to quantify the desired amount of target molecule even with the naked-eye readout. The approach is based on the use of red-fluorescent CdSe@ZnS QDs (655-QDs) that are modified with target-specific antibodies (**Figure 1**). At the same time, target-independent blue fluorescent polystyrene nanobeads (450-NBs) are immobilized on the test line (TL) together with target-specific antibodies. The presence of the target and the subsequent immune-sandwich formation induces the accumulation of the 655-QDs on the TL. The co-localization of red and blue fluorescent labels on the TL generates a wide color palette (including red, pink, purple, and blue). Importantly, since the amount of 450-NBs is controlled during the fabrication of the LFA, we can associate a specific color to a specific target concentration and, therefore, modulate the dynamic range of the LFA. We believe that our ratiometric approach will facilitate the development of new LFAs by easily tuning their dynamic range upon the particular requirements of each application.
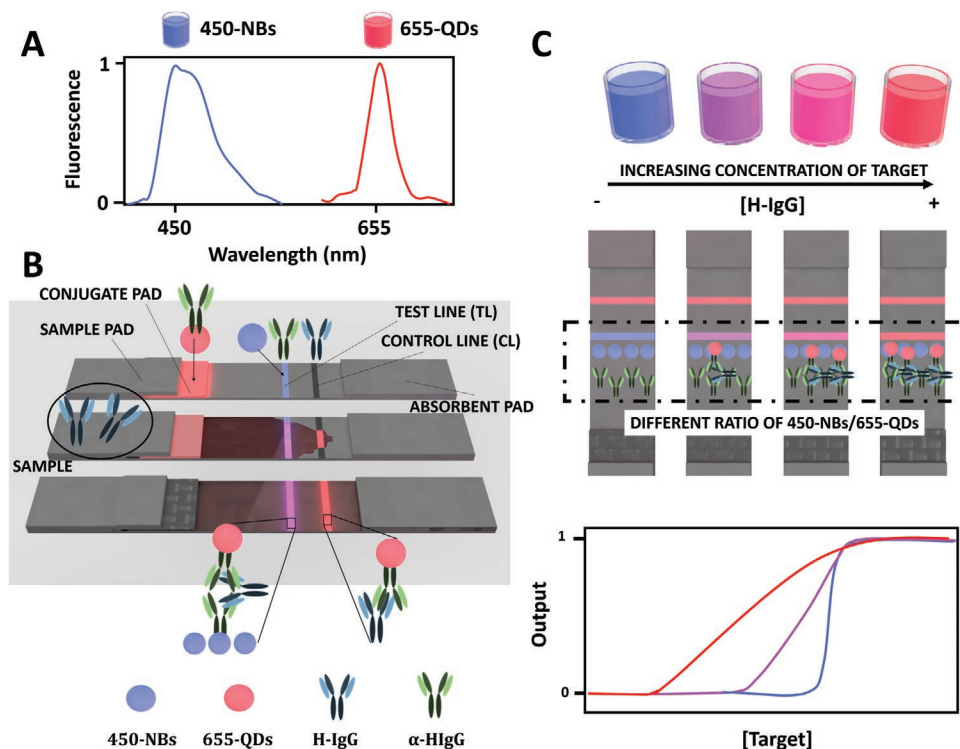

Figure 1. A) Wavelength emission spectra of the 450-NBs and 655-QDs labels, showing a maximum emission peak at 450 and 655 nm, respectively. B) Schematic representation of the ratiometric LFA strip for H-IgG detection. 655-QDs (red nanoparticles) are conjugated to α-HIgG antibodies and placed on the conjugate pad, while unmodified 450-NBs (blue nanoparticles) are preadsorbed together with α-HigG antibodies on the TL. H-IgG antibodies are deposited on the CL. The presence of the target analyte in the sample promotes the formation of the immune-complex on the TL, generating a progressive color change from blue to purple, pink and red, which can be quantitatively related to the concentration of the target analyte. C) The combination of different ratios of 450-NBs and 655-QDs leads to the modulation of the assay's dynamic range.

2101450 (2 of 9)

2. Results and Discussion

2.1. Concept

We propose the application of a ratiometric strategy in LFA exploiting red-fluorescent 655-QDs (as target-dependent signal transducers) and blue fluorescent 450-NBs (as target-independent reporters) (Figure 1A). The formers are functionalized with anti-HIgG antibodies and located on the conjugate pad, while the latter are not modified, and they are placed on the TL together with anti-HIgG antibodies (Figure 1B). The presence of the target (i.e., H-IgG) promotes the accumulation of the antibody-conjugated 655-QDs on the TL, leading to the co-localization of the two fluorescent labels on the TL. This induces a color change on the TL that depends on the concentration of the target analyte in the sample. That is, for increasing concentrations of target the color signal will progressively shift from blue to pink, purple, and finally red. Conversely, the absence of the target in the sample will keep the blue fluorescence emission in the TL. In both cases, the control line (CL) (based on secondary antibodies specific for those on the surface of 655-QDs) will always provide a red fluorescence signal, indicating that the assay has properly worked (Figure 1B,C).

The ability to control the dynamic range of our LFA depends on two parameters: 1) the color tonality of TL which depends on the red/blue fluorescent ratio, and 2) the amount of 450-NBs on the TL which can be controlled during its deposition. Regarding the former, since each color of our palette is associated with a specific red/blue ratio, the two labels must increase or decrease accordingly to always obtain the desired color. Specifically, the more 450-NBs on the TL, the more 655-QDs are required to produce the same color shift. Regarding the latter, we can vary the amount of 450-NBs on the TL to precisely obtain the

desired color for a specific target concentration. For example, assuming the fluorescence signals of the two labels equally change with changes in their concentration, if we want to shift the dynamic range of the LFA one order of magnitude, we can simply deposit on the TL tenfold the amount of 450-NBs. In this way, it would be required tenfold the amount of target to accumulate enough 655-QDs to compensate for the increased amount of 450-NBs. This precise control of the dynamic range allows us to quantify the desired amount of target with the naked eye. At the same time, it allows also to easily avoid the hook effect,[48] which is the loss of signal intensity in the test line upon the presence of excess target analyte in the sample (the consequent low signal intensity can be falsely interpreted as a low target analyte concentration).

2.2. Nanoparticles Characterization

To develop our ratiometric LFA we selected two fluorescent labels (655-QDs and 450-NBs) which display the same excitation wavelength, but different emission spectra (**Figure 2**A). Of note, as excitation source we choose an ultraviolet (UV) LED because it emits light at a wavelength of 365 nm and it is suitable for point-of-care applications (i.e., it is cost-effective (0.85€) and portable (5 mm)). Upon excitation of the labels at 365 nm we collected the maximum emission peaks at 450 and 655 nm for the 450-NBs and 655-QDs, respectively (Figure 2A). Next, we characterized the fluorescence color variations when mixing the nanoparticles at different ratios in solution. Specifically, we started identifying the concentrations that provide an equal fluorescence signal intensity (Figure 2B, purple spectrum). This was achieved by using a solution with 0.32% 655-QDs and 450-NBs at 0.45% (w/v), which was related to a red emission peak of 2.9E+08 a.u. and a blue emission peak of 2.7E+08 a.u.
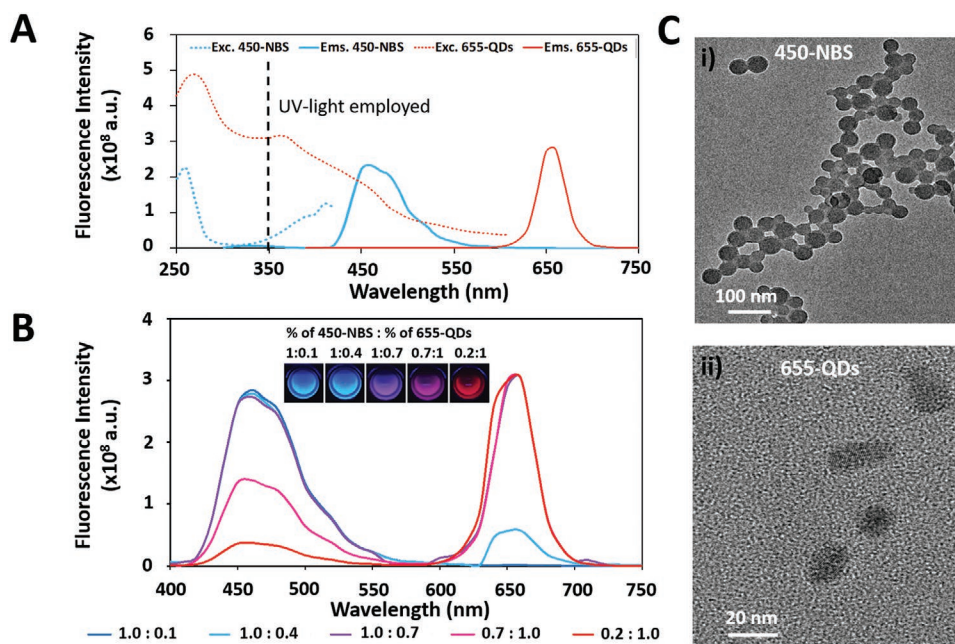

Figure 2. A) Excitation and emission spectra of the 450-NBs (0.45%) and 655-QDs (0.32%). B) Emission spectra resulting from the ratiometric combinations of the 450-NBs and the 655-QDs. Inset of the emitted fluorescence under the UV lamp. C) TEM images of the i) 450-NBs and ii) 655-QDs.

With this combination, we obtained a purple fluorescent signal (Figure 2B). The next step was to vary these concentrations to generate color changes. Specifically, to obtain a pink fluorescent signal we kept the concentration of 655-QDs at 0.32% and we diluted to half (0.225%) the concentration of 450-NBs. This was related to a red emission peak of 2.9E+08 a.u. and a blue emission peak of 1.4E+08 a.u. Finally, using 0.32% of 655-QDs and the 450-NBs at 0.056% we have suppressed the blue signal obtaining the expected red fluorescence. This was related to a red emission of 3.0 E+8 a.u. and a blue emission of 3.8 E+7 a.u. The collected data demonstrate that we can generate four different colors (blue, pink, purple, red) by simply changing the relative amounts of 450-NBs and 655-QDs, suggesting the feasibility of the ratiometric approach using these two fluorescent nanoparticle labels.

Besides having a strong measurable optical signal, the ideal label of a LFA must flow through the nitrocellulose membrane and be stable enough to be dried on the conjugate pad without aggregating. Therefore, we characterized the size and dispersity of the nanoparticles using transmission electron microscopy (TEM), which can provide a good indication of the particle size and dispersity. As we can observe in Figure 2C-i 450-NBs display a diameter of 43.3 ± 5.6 nm (in agreement with the one specified by the company)[49]; however they tend to aggregate into clusters of up to 2 μm, limiting their ability to move along the CNPF200 nitrocellulose membrane (with a pore size of 5 μm). Since their inability to move guarantees a stable blue signal for the whole duration of the assay, we used them as target-independent label printed directly on the TL (Figure S1, Supporting Information). On the contrary, the 655-QDs display a diameter of 17.5 ± 2.5 nm and they do not show any indication of being prone to aggregation. Therefore, we used them as the target-dependent label since they can easily move along the nitrocellulose membrane (see Figure 2C-ii).

2.3. Ratiometric Concept on Paper Substrate

To adapt our proposed approach to a LFA, we characterized the ratiometric optical signal using nitrocellulose (the material commonly used as a detection pad of LFAs) and a smartphone camera (the ideal point-of-care optical reader).[50] Generally, there are two main color models used to quantify images: RGB and HSB.[51] In RGB, colors are represented by the combination of the three primary colors Red, Green, and Blue described by a numerical scale from 0 to 255. Instead, the HSB model represents a color by its Hue (H), its Saturation (S), and Brightness (B). The Hue values are generally based on a 360° color wheel, where 0, 120°, and 240° are related to red, green, and blue, respectively. This latter system conceives colors more like the human eye does.[52] That is, the HSB model (and in particular the Hue) relates a color tonality with a single numerical value, simplifying the quantification of color variations in LFA. In contrast, the RGB model is better suited to analyze color intensity, as it enables an independent quantification of the three primary colors.[53] For instance, when analyzing the accumulation of 655-QDs on the TL of a non-ratiometric LFA, the parameter of interest is the R value, since the G and B values remain constant. Therefore, in our work we used both color scales, the HSB model to measure ratiometry-based LFA and the RGB to measure LFA relying on a single optical label. Importantly, while the HSB values range from 0 to 360, since we rely on the ImageJ's "HSB stack" tool the values change between 0 and 255 (Figure S2, Supporting Information).[54] In the case of the fluorescent labels employed in this study, we obtained H values of 241° and 235° for 655-QDs in solution and on nitrocellulose, respectively; and H values of 147° and 148° for 450-NBs in solution and on nitrocellulose, respectively. As observed, there is no significant difference between the H values obtained in solution and in nitrocellulose, which highly supports the applicability of these nanoparticles in ratiometric strategies on paper-based platforms.

We then proceeded to further demonstrate the applicability of the ratiometric approach on a paper-like substrate, using a smartphone camera as a reader. That is, testing different combinations of 655-QDs and 450-NBs directly on the nitrocellulose. Of note, since 450-NBs tend to create a coffee ring effect on the paper during the data analysis we only considered the central part of the line (Figure S2, Supporting Information). As expected, we achieved the same color palette both on nitrocellulose and in solution (**Figure 3**A). For example, using 0.04% of
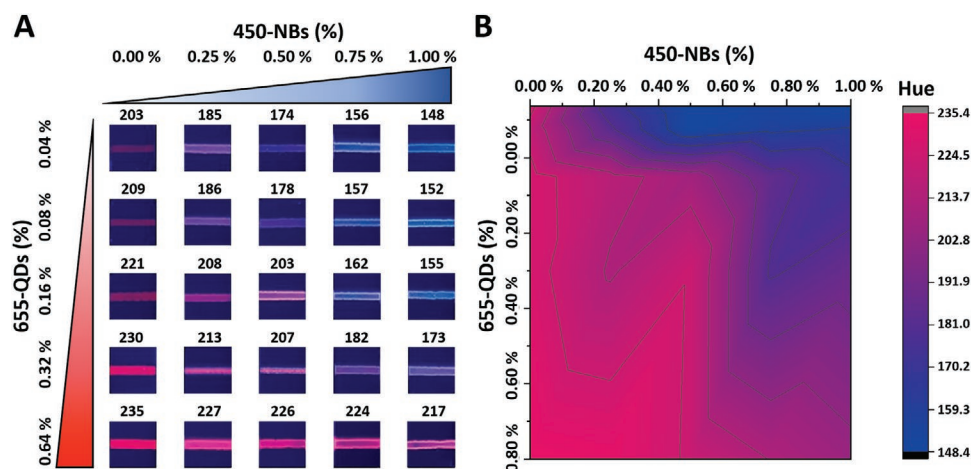

Figure 3. A) Color combination of different concentrations of 655-QDs (0.64%, 0.32%, 0.16%, 0.08%, 0.04%) and 450-NBs (1%, 0.75%, 0,5%, 0,25%, 0%) on the nitrocellulose (CNPF200). B) Color map representing the hue value of the different combinations of 655-QDs and 450-NBs.

**ADVANCED
SCIENCE NEWS**
www.advancedsciencenews.com

**ADVANCED
MATERIALS
TECHNOLOGIES**
www.advmattechnol.de

the 655-QDs and the 450-NBs at a concentration of 0.25% we could obtain purple (H value of 185). Instead, using 0.16% of the 655-QDs and the 450-NBs at a concentration of 0.25% we could obtain pink (H value of 208). Exploiting this data, we built a map (Figure 3B) to better represent and explain the influence of the different concentrations of fluorescent labels on the final color. Observing the map, it is clear that the higher the concentration of 655-QDs, the more 450-NBs are required to induce a color change. Specifically, while using 0.16% of 655-QDs we can observe all the possible colors (red > pink > purple > blue) by increasing the amount of 450-NBs, using 0.64% of 655-QDs inhibited the color shift even using the highest amount of 450-NBs.

2.4. Design of the Ratiometric LFA

We decided to apply the ratiometric approach to precisely tune the dynamic range of LFAs. Since the final TL color depends on the red/blue ratio, we can control the concentration of analyte that will induce the desired color change based on the amount of 450-NBs we pre-deposit on the TL. To prove this, we printed

on the nitrocellulose membrane different amounts of 450-NBs: 1.0%, 0.1%, 0.01%, and 0%. Then we performed calibration curves using concentrations of the target (H-IgG) between 0 to 1000 ng mL^{-1} (which corresponds to 6.6×10^{-9} M) (**Figure 4**A). The formation of the immune-sandwich complex induces the accumulation of the 655-QDs on the TL producing the desired color change. Of note, for this set of experiments we modified the conjugate pad with a solution of anti-HIgG-conjugated 655-QDs at 0.16% because it provides a good compromise between cost-effectiveness and a visible optical signal by the naked eye.

Looking at the results obtained in the absence of 450-NBs we observe that the LFA responded as expected. That is, increasing concentrations of H-IgG produce a more intense red TL. In this case, since there is no 450-NBs on the TL, there is no color change, but just an increasing color intensity (as for classical LFAs) that starts to be appreciable by naked eye at 63.10 ng mL^{-1} of H-IgG and it saturates at 398.1 ng mL^{-1} of H-IgG (Figure 4A). Conversely, the results obtained using strips with pre-adsorbed 450-NBs on the TL confirm that the ratiometric approach can indeed be used to tune the LFA's dynamic range. For instance, when fixing 0.01% of 450-NBs on TL, the first color change from blue to purple can be visualized upon the detection of
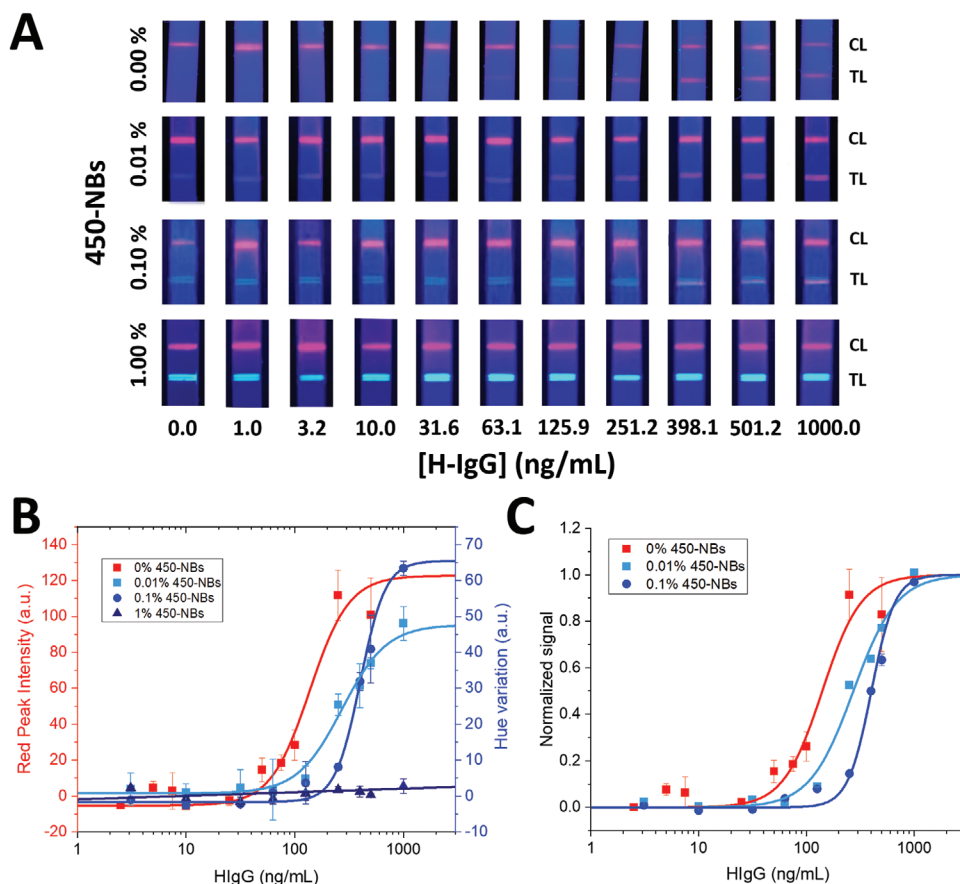

Figure 4. A) Picture of the LFA strips with 0.00%, 0.01%, 0.10%, and 1.00% 450-NBs in TL, after performing the calibration curve for the detection of H-IgG (0–1000 ng mL^{-1}) in PBS buffer. B) Quantification of the red peak intensity variation (left y-axis) of the non-ratiometric LFA strips (0.00% 450-NBs in TL) and the Hue variation (right y-axis) after performing the calibration curve for the detection of H-IgG (0–1000 ng mL^{-1}) using the ratiometric LFA strips with 0.01%, 0.10%, and 1.00% 450-NBs in TL. Data of the curves fitting is shown in Table S2 (Supporting Information). C) Calibration curves showing the normalized red peak intensity variation of the non-ratiometric LFA strips and the normalized Hue variation for the ratiometric strips with 0.01% and 0.10%. Data of the curves fitting is shown in Table S3 (Supporting Information).

31.6 ng mL^{-1} of H-IgG, the second color change from purple to pink occurs when detecting 125.9 ng mL^{-1}, and the third color change from pink to red is perceived at 1000 ng mL^{-1} of H-IgG. Therefore, with the simple pre-adsorption of 450-NBs on the TL, we can shift the linear dynamic range to higher concentrations of the target analyte. The dynamic range can be further displaced to the right by raising the amount of 450-NBs on the TL. For example, the use of 0.1% of 450-NBs promotes a delay in the generation of the first and second color changes, which occur at 398.1 and 1000 ng mL^{-1} of H-IgG (Figure 4A). Following the same trend, no color change can be observed within the range of 0–1000 ng mL^{-1} of H-IgG when using 1% of 450-NBs on TL (Figure 4A).

We then proceeded with the quantification of the results. In the case of the non-ratiometric LFA, for the quantification of the signal, we cannot rely on the H value (since it measures color change) (Figure S3, Supporting Information), but instead, we used a previously reported method based on the measurement of the RGB pixels and their conversion to brightness values.[23] Regarding the ratiometric LFA, we used the H value since the output is not the intensity of the TL, but the color change (Figure S2, Supporting Information). The collected data can be fitted to a 4-parameter logistic (sigmoidal) equation. Figure 4B compares the H value variation of the three ratiometric conditions with the red peak intensity variation of the non-ratiometric LFA. Of note, to better observe the signal variation we subtracted the baseline from the curves obtained for 0.01%, 0.1%, and 1% 450-NBs. Instead, Figure 4C shows the same data but normalized, in this way it is easier to compare the shift in the dynamic range among the different LFAs tested.

To better explain and estimate the different dynamic ranges, we have compared the inflection point and Hill coefficient of each calibration curve (see **Table 1**). The former provides information regarding the dynamic range of the curve (i.e., the target concentration corresponding to the half of the maximum signal), while the latter enables the quantification of the assay's sensitivity, as it is related to the steepness of the calibration curve slope. As expected, the application of ratiometry and the subsequent increase of the 450-NBs concentration on the TL promotes the progressive increase of the inflection point in the calibration curve, which in turn results in a shift of the dynamic range toward higher concentrations of the analyte. For instance, almost a twofold and threefold increase in the inflection point is achieved when depositing 0.01 (Figure 4C, light

blue curve) and 0.1% more concentration of 450-NBs on the TL (Figure 4C, blue curve). Similarly, the Hill coefficient increases 1.8-fold (3.99) when depositing tenfold more 450-NBs on the TL. This is because when fixing a higher concentration of 450-NBs on the TL, more concentration of target is required to increase the Hue value, which in turn increases faster at higher target analyte concentrations.[55] Therefore, the combination of 0.16% 655-QDs and 0.1% 450-NBs provides a 1.8-fold sensitivity enhancement compared to the combination of the same concentration of 655-QDs and tenfold lower concentration of 450-NBs.

2.5. Applicability with Complex Samples

Finally, we tested the applicability of the ratiometric strategy using an undiluted and untreated serum. Serum samples are known to interfere with the signal generated on the TL, by masking the optical signal due to their intrinsic opacity and/ or by hindering the immunorecognition of the target analyte due to the presence of competing protein-based molecules.[56] To prove the compatibility of the proposed biosensor with complex samples we spiked H-IgG into fetal bovine serum (FBS). We performed the calibration curves using the same concentrations of fluorescence labels and analyte as in the previous experiment, and we observed the same trend. Specifically, the signal achieved on the TL when evaluating a blank serum sample (without the spiked H-IgG) was significantly similar to the signal obtained when analyzing a blank PBS sample. Thus, there was no interference between the antibodies used as bioreceptors and the biomolecules of the serum sample. In addition, the signal intensity in TL was not masked by the FBS and the color tonalities were not affected for all the evaluated conditions (Figure S4, Supporting Information). Analyzing the collected data, we achieved a Hill coefficient of 1.52 and an inflection point of 79.29 ng mL^{-1}, resulting in a dynamic range of 5 to 300 ng mL^{-1} for 0% 450 NBs (see Table 1). Whereas we achieved a Hill coefficient of 2.39 and an inflection point of 120.14 ng mL^{-1}, giving a dynamic range of 30 to 400 ng mL^{-1} for 0.1% 450 NBs (**Figure 5**). Therefore, the same trend is observed when evaluating a more complex sample matrix such as fetal bovine serum, where both a higher inflection point, and Hill coefficient are achieved when using the ratiometric LFA with 0.16% 655-QDs and 0.1% 450-NBs.

3. Final Remarks and Conclusions

In this study, we have developed a simple and cost-effective approach to modulate the dynamic range and sensitivity of LFAs through the application of a ratiometric strategy based on target-dependent fluorescent QDs (655-QDs) and target-independent polystyrene nanobeads (450-NBs). Firstly, we have demonstrated the ratiometric capability of these labels in solution, where the expected color change from blue to red can be achieved only by changing the concentration ratios of each nanoparticle. We have then proved the ratiometric strategy on a paper-based substrate. More specifically, the same color tonalities (obtained in solution) can be perceived when the
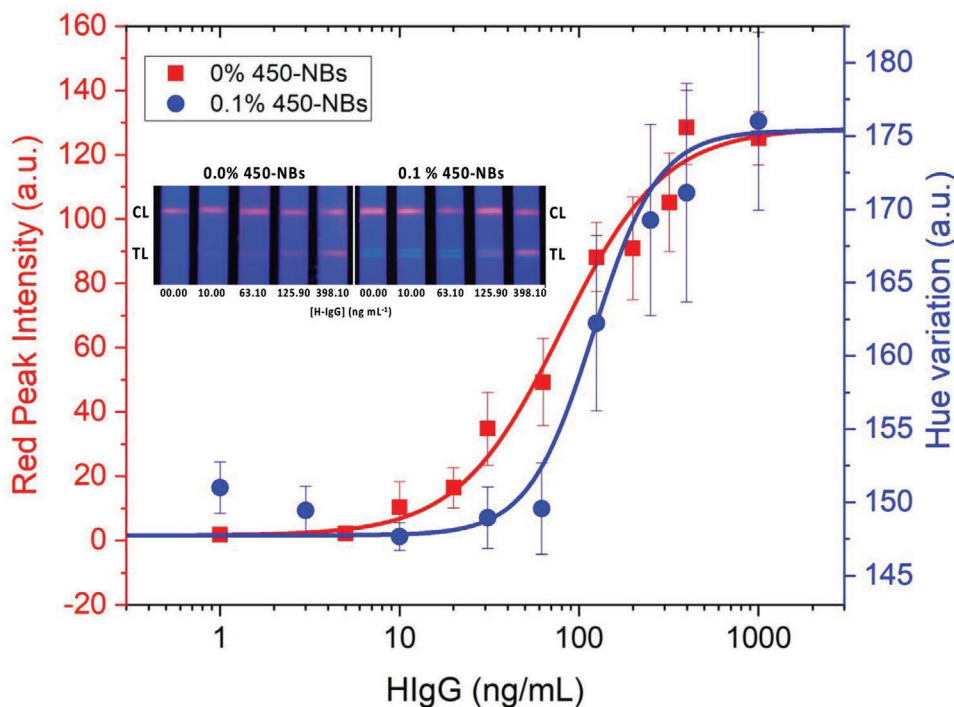
Table 1. Comparison of the analytical parameters of the ratiometric and non-ratiometric LFA for H-IgG detection in PBS buffer and FBS.

% 450-NBs	Hill coefficient	Inflection point [ng mL^{-1}]	Dynamic range [ng mL^{-1}]
Calibration curve in PBS buffer			
0.00	2.40	137.55	56–300
0.01	2.16	272.89	100–700
0.10	3.99	401.11	112–700
Calibration curve in FBS			
0.00	1.52	79.29	5–300
0.10	2.39	120.14	30–400

Figure 5. Red peak intensity and Hue variation along the calibration curve for H-IgG detection (0–1000 ng mL^{-1}) in FBS samples using non-ratiometric and ratiometric LFA strips with 0.1% of 450-NBs on the TL. Inset of the LFA strips with 0.0%, 0.1% of 450-NBs after the detection of 0.00, 10.00, 63.10, 125.90, and 398.10 ng mL^{-1}. Data of the curves fitting is shown in Table S4 (Supporting Information).

fluorescent labels are located on the nitrocellulose membrane resulting in the expected wide color palette (blue, purple, pink, and red). To better understand this, we have created a color map based on the hue values and we demonstrated that the variation in the color tonality can be modulated upon the combination of the labels at different ratios. Finally, by applying this concept in a LFA, we have shown that a gradual shift of the dynamic range can be achieved upon the pre-adsorption of higher concentrations of 450-NBs on the TL. We have also observed that the application of ratiometry provides a sensitivity enhancement when evaluating the assay qualitatively with the naked eye. Compared to the already reported analytical methods for H-IgG detection, our approach provides a 78-fold higher analytical sensitivity, an 18-fold faster assay time (compared to ELISA) and the possibility to progressively shift the dynamic range, which is something inconceivable in conventional LFAs (Table S5, Supporting Information). Looking ahead, we envisage that our ratiometric approach could benefit from solutions addressing issues common to all fluorescence based LFAs. For example, by employing better cut-off filters, more defined excitation light sources (with narrower emission peak) and up-converting fluorescent labels (with NIR excitation), it should be possible to decrease the background noise and therefore improve the sensitivity, specificity and LoD of the assay.

The results described in this work demonstrate how the proposed ratiometric approach can be used as a new tool to precisely control the assay's dynamic range and to improve the sensitivity in LFA (see Table S1, Supporting Information). For example, during the development of a LFA its analytical properties can be easily tuned (without selecting novel bioreceptors or membranes) to receive approval from regulatory agencies. Or, in case of an already existing LFA that needs to be adapted for a new application, its sensitivity and dynamic range can also be adapted with minor modification on the fabrication process (again without the need to select new bioreceptors or membranes). We believe that the ratiometric approach proposed in this manuscript has the potential to dramatically affect the way LFAs are designed and developed saving precious resources and providing the public with better and more readily available point-of-care sensors.

4. Experimental Section

Materials and Reagents: Human IgG antibody, goat anti-human IgG, bovine se-rum albumin (BSA), phosphate buffer saline (PBS) tablets, sucrose, and tween 20 were purchased from Sigma Aldrich (Madrid, Spain). Nitrocellulose membrane CNPF200 was purchased from mdi (Ambala Cantt, India). Cellulose membrane (CFSP001700) was purchased from Merck Millipore (Billerica, MA, USA), glass fiber Standard 14 was purchased from GE Healthcare (Chicago, IL, USA) and the supporting adhesive cards were purchased from Kenosha (Amstelveen, The Netherlands). Fluoro-Max Dyed Blue Aqueous Fluorescent Particles (450-NBs), Qdot 655 and Qdot 655 goat F(ab')2 anti-human IgG conjugate (H+L) (655-QDs) were purchased from Thermo Fisher Scientific (Eugene, OR, USA). Fetal Bovine Serum (FBS) was purchased from Linus (Madrid, Spain).

Instruments: The IsoFlow Bioreagent dispenser and the lateral flow strips cutter used for the fabrication of the strips were purchased from Imagene Technology (Hanover, Germany) and Shanghai Kinbio Tech (Pudong New District, Shanghai, China), respectively. The spectrophotometer SpectraMax ID3 and transmission electron microscope TEM Technai F20 used for the characterization of the nanoparticles were purchased from

Molecular devices (San Jose, CA, USA) and (Hillsboro, OR, USA). The Smartphone Xiaomi Redmi Note 8 used for the assay evaluation was purchased from Xiaomi (Beijing, China).

Nanoparticles Characterization: The excitation and emission spectra of the Fluoro-Max dyed blue aqueous fluorescent particles (450-NBs) and the CdSe@ZnS quantum dots (655-QDs) were evaluated with the SpectraMax ID3 spectrophotometer, while the size and shape distribution of the nanoparticles were characterized using the Technai F20 TEM.

LFA Strips Fabrication: The functionalization of the detection pad was always conducted with the nitrocellulose membrane immobilized on a supporting laminated card. Firstly, the nitrocellulose CNPF200 membrane was functionalized with a solution containing 450-NBs (depending on the experimental condition the concentration changed between 0% and 0.1% in PBS buffer 10×10^{-3} M pH 7.4) on the test line (TL). Once fixed-dried at 37 °C for 2 h, a solution of anti-HIgG (1 mg mL^{-1}) and H-IgG (1 mg mL^{-1}) in PBS buffer 10×10^{-3} M pH 7.4 was deposited on the TL and control line (CL) and dried at 37 °C for 2 h. Both the 450-NBs and the antibody solutions were dispensed using the bioreagent dispenser at a flow rate of 0.5 µL cm^{-1} and using a speed of 50 mm s^{-1}. The conjugate solution was prepared by diluting the 655-QDs modified with goat F(ab')2 anti-human IgG conjugate solution to 0.16% (w/v) using PBS buffer (10×10^{-3} M pH 7.4, 1% BSA, 0.5% Tween 20 and 10% sucrose), then the solution was drop-casted on the glass fiber membrane and dried in a vacuum chamber at room temperature for 1.5 h. Cellulose membrane was used as sample and absorbent pad. For the sample pad the cellulose membrane was first soaked into sample pad buffer (PBS buffer containing 0.5% (wt/vol) BSA and 0.05% (vol/vol) Tween-20) and then dried at 37 °C for 2 h, before mounting it on the laminated card. The laminated card was cut into 3 mm width strips using an automatic cutter.

H-IgG Detection and Assay Evaluation: The calibration curve was performed by drop-casting 100 µL of known concentrations of H-IgG (from 0 to 1 µg mL^{-1} in PBS buffer 10×10^{-3} M pH 7.4 and spiked FBS) on the sample pad. The strips were incubated at room temperature for 10 min on a table covered with a black matte cardboard. This was used to prevent light reflection during the assay evaluation. The results were recorded by taking a picture with the smartphone (48 megapixels), 10 min after the sample addition, by keeping a 9 cm distance from the strips and under constant illumination conditions. The camera parameters of the smartphone were manually set to ISO speed (100) and shutter speed (1/4 s). UV LEDs were used to excite the fluorescent nanoparticles at a wavelength of 365 nm.

The pictures were analyzed using the open-source Image J software,[57] which enables the quantification of both the color intensity and the color variation. Specifically, the measurement of the color intensity was done following the recently published protocol.[25] Briefly, after splitting the image into the three different RGB channels, a plot profile (covering the total width of the nitrocellulose membrane) for each LFA was measured just for the red channel. The peak height was then measured and used to analyze the sensor performance. In the case of measuring the color variation, each image was transformed using the HSB stack feature. Then the plot profile for the Hue (H) feature was analyzed for each strip. The peak value was recorded and used for the analysis. Note that while for the color intensity the peak height (i.e., peak value – baseline) was measured, for the color variation just the peak value was measured, since it corresponds to the color seen by the naked eye. In order to facilitate the comparison between different LFAs and conditions, in the manuscript normalized data (min–max normalization) was also presented.[58] The limit of detection (LoD) was calculated as Optical intensity (LoD) = blank + 3 σ blank (i.e., the corresponding value of blank sample plus 3 times its standard deviation). The limit of quantification (LoQ) was calculated as Optical intensity (LoQ) = blank + 10 σ blank.[59]

Supporting Information

Supporting Information is available from the Wiley Online Library or from the author.

Conflict of Interest

The authors declare no conflict of interest.

Data Availability Statement

The data that support the findings of this study are available from the corresponding author upon reasonable request.

[1] K. J. Land, D. I. Boeras, X. S. Chen, A. R. Ramsay, R. W. Peeling, *Nat. Microbiol.* **2019**, *4*, 46.

[2] P. Brangel, A. Sobarzo, C. Parolo, B. S. Miller, P. D. Howes, S. Gelkop, J. J. Lutwama, J. M. Dye, R. A. McKendry, L. Lobel, M. M. Stevens, *ACS Nano* **2018**, *12*, 63.

[3] D. Quesada-González, G. A. Jairo, R. C. Blake, D. A. Blake, A. Merkoçi, *Sci. Rep.* **2018**, *8*, 16157.

[4] A. Sena-Torralba, Y. Pallás-Tamarita, S. Morais, Á. Maquieira, *TrAC, Trends Anal. Chem.* **2020**, *132*, 116050.

[5] C. Parolo, A. Merkoçi, *Chem. Soc. Rev.* **2013**, *42*, 450.

[6] X. Huang, Y. Liu, B. Yung, Y. Xiong, X. Chen, *ACS Nano* **2017**, *11*, 5238.

[7] B. D. Grant, C. E. Anderson, J. R. Williford, L. F. Alonzo, V. A. Glukhova, D. S. Boyle, B. H. Weigl, K. P. Nichols, *Anal. Chem.* **2020**, *92*, 11305.

[8] X. Huang, Z. P. Aguilar, H. Xu, W. Lai, Y. Xiong, *Biosens. Bioelectron.* **2015**, *75*, 166.

[9] "Pregnancy Tests," can be found under https://uk.clearblue.com/pregnancy-tests, **2020**.

[10] D. Wang, S. He, X. Wang, Y. Yan, J. Liu, S. Wu, S. Liu, Y. Lei, M. Chen, L. Li, J. Zhang, L. Zhang, X. Hu, X. Zheng, J. Bai, Y. Zhang, Y. Zhang, M. Song, Y. Tang, *Nat. Biomed. Eng.* **2020**, *4*, 1150.

[11] T. Nicol, C. Lefeuvre, O. Serri, A. Pivert, F. Joubaud, V. Dubée, A. Kouatchet, A. Ducancelle, F. Lunel-Fabiani, H. Le Guillou-Guillemette, *J. Clin. Virol.* **2020**, *129*, 104511.

[12] A. Sena-Torralba, D. B. Ngo, C. Parolo, L. Hu, R. Álvarez-Diduk, J. F. Bergua, G. Rosati, W. Surareungchai, A. Merkoçi, *Biosens. Bioelectron.* **2020**, *168*, 112559.

[13] T. Shaw, C. Tellapragada, K. E. Vandana, D. P. AuCoin, C. Mukhopadhyay, *PLoS One* **2018**, *13*, e0194595.

[14] A. Scohy, A. Anantharajah, M. Bodéus, B. Kabamba-Mukadi, A. Verroken, H. Rodriguez-Villalobos, *J. Clin. Virol.* **2020**, *129*, 104455.

[15] C. Wang, C. Wang, X. Wang, K. Wang, Y. Zhu, Z. Rong, W. Wang, R. Xiao, S. Wang, *ACS Appl. Mater. Interfaces* **2019**, *11*, 19495.

[16] B. S. Miller, L. Bezinge, H. D. Gliddon, D. Huang, G. Dold, E. R. Gray, J. Heaney, P. J. Dobson, E. Nastouli, J. J. L. Morton, R. A. McKendry, *Nature* **2020**, *587*, 588.

[17] A. Sena-Torralba, R. Álvarez-Diduk, P. Claudio, T.-M. Helena, A. Müller, A. Merkoçi, *Anal. Chem.* **2021**, *93*, 3112.

[18] L. Rivas, M. Medina-Sánchez, A. de la Escosura-Muñiz, A. Merkoçi, *Lab Chip* **2014**, *14*, 4406.

[19] Z. Qu, K. Wang, G. Alfranca, J. M. de la Fuente, D. Cui, *Nanoscale Res. Lett.* **2020**, *15*, 10.

[20] B. S. Miller, C. Parolo, V. Turbé, C. E. Keane, E. R. Gray, R. A. McKendry, *Chem. - Eur. J.* **2018**, *24*, 9783.

[21] N. Amin, A. Sena-Torralba, R. Álvarez-Diduk, A. Afkhami, A. Merkoçi, *Anal. Chem.* **2020**, *92*, 4209.

[22] Y. Liu, L. Zhan, Z. Qin, J. Sackrison, J. C. Bischof, *ACS Nano* **2021**, *15*, 3593.

[23] J. F. Bergua, L. Hu, C. Fuentes-Chust, R. Álvarez-Diduk, A. H. A. Hassan, C. Parolo, A. Merkoçi, *Lab Chip* **2021**, *21*, 2417.

[24] D. Quesada-González, A. Sena-Torralba, W. P. Wicaksono, A. de la Escosura-Muñiz, T. A. Ivandini, A. Merkoçi, *Biosens. Bioelectron.* **2019**, *132*, 132.

[25] C. Parolo, A. Sena-Torralba, J. F. Bergua, E. Calucho, C. Fuentes-Chust, L. Hu, L. Rivas, R. Álvarez-Diduk, E. P. Nguyen, S. Cinti, D. Quesada-González, A. Merkoçi, *Nat. Protoc.* **2020**, *15*, 3788.

[26] W. Xiao, C. Huang, F. Xu, J. Yan, H. Bian, Q. Fu, K. Xie, L. Wang, Y. Tang, *Sens. Actuators, B* **2018**, *266*, 63.

[27] C. Ruppert, N. Phogat, S. Laufer, M. Kohl, H. P. Deigner, *Microchim. Acta* **2019**, *186*, 119.

[28] H. Wang, L. Yang, S. Chu, B. Liu, Q. Zhang, L. Zou, S. Yu, Changlong Jiang, *Anal. Chem.* **2019**, *91*, 9292.

[29] S. Chu, H. Wang, X. Ling, S. Yu, L. Yang, Changlong Jiang, *ACS Appl. Mater. Interfaces* **2020**, *12*, 12962.

[30] S. Chu, H. Wang, Y. Du, F. Yang, L. Yang, Changlong Jiang, *ACS Sustainable Chem. Eng.* **2020**, *8*, 8175.

[31] D. A. Mendels, L. Dortet, C. Emeraud, S. Oueslati, D. Girlich, J. B. Ronat, S. Bernabeu, S. Bahi, G. J. H. Atkinson, T. Naas, *Proc. Natl. Acad. Sci. USA* **2021**, *118*, e2019893118.

[32] A. Carrio, C. Sampedro, J. L. Sanchez-Lopez, M. Pimienta, P. Campoy, *Sensors* **2015**, *15*, 29569.

[33] D. Gasperino, T. Baughman, H. V. Hsieh, D. Bell, B. H. Weigl, *Annu. Rev. Anal. Chem.* **2018**, *11*, 219.

[34] A. Bigdeli, F. Ghasemi, S. Abbasi-Moayed, M. Shahrajabian, N. Fahimi-Kashani, S. Jafarinejad, M. A. Farahmand Nejad, M. R. Hormozi-Nezhad, *Anal. Chim. Acta* **2019**, *1079*, 30.

[35] P. Wu, X. Hou, J. J. Xu, H. Y. Chen, *Nanoscale* **2016**, *8*, 8427.

[36] Y. Zhou, X. Huang, C. Liu, R. Zhang, X. Gu, G. Guan, C. Jiang, L. Zhang, S. Du, B. Liu, M. Y. Han, Z. Zhang, *Anal. Chem.* **2016**, *88*, 6105.

[37] X. Huang, Y. Xiong, J. Song, B. C. Yung, X. Chen, X. Huang, *Chem. Soc. Rev.* **2018**, *47*, 2873.

[38] P. T. Snee, R. C. Somers, G. Nair, J. P. Zimmer, M. G. Bawendi, D. G. Nocera, *J. Am. Chem. Soc.* **2006**, *128*, 13320.

[39] C. M. Tyrakowski, P. T. Snee, *Anal. Chem.* **2014**, *86*, 2380.

[40] J. Lee, M. B. Brennan, R. Wilton, C. E. Rowland, E. A. Rozhkova, S. Forrester, D. C. Hannah, J. Carlson, E. V. Shevchenko, D. S. Schabacker, R. D. Schaller, *Nano Lett.* **2015**, *15*, 7161.

[41] X. Wang, S. Yu, W. Liu, L. Fu, Y. Wang, J. Li, L. Chen, *ACS Sens.* **2018**, *3*, 378.

[42] K. He, X. Zhan, L. Liu, X. Ruan, Y. Wu, *Photochem. Photobiol.* **2020**, *96*, 1154.

[43] Z. Luo, T. Lv, K. Zhu, Y. Li, L. Wang, J. J. Gooding, G. Liu, B. Liu, *Angew. Chem., Int. Ed.* **2020**, *59*, 3131.

[44] C. Liu, D. Ning, C. Zhang, Z. Liu, R. Zhang, J. Zhao, T. Zhao, B. Liu, Z. Zhang, *ACS Appl. Mater. Interfaces* **2017**, *9*, 18897.

[45] J. Wang, C. Jiang, J. Jin, L. Huang, W. Yu, B. Su, J. Hu, *Angew. Chem., Int. Ed.* **2021**, *100193*, 13042.

[46] K. G. Shah, V. Singh, P. C. Kauffman, K. Abe, P. Yager, *Anal. Chem.* **2018**, *90*, 6967.

[47] L. Li, Y. Zhang, S. Ge, L. Zhang, K. Cui, P. Zhao, M. Yan, J. Yu, *Anal. Chem.* **2019**, *91*, 10273.

[48] G. M. S. Ross, D. Filippini, M. W. F. Nielen, G. I. J. Salentijn, *Anal. Chem.* **2020**, *92*, 15587.

[49] ThermoFischer Scientific, "Fluoro-Max B0100," can be found under https://www.thermofisher.com/order/catalog/product/B0100#/B0100, **2021**.

[50] J. Liu, Z. Geng, Z. Fan, J. Liu, H. Chen, *Biosens. Bioelectron.* **2019**, *132*, 17.

[51] J. L. D. Nelis, L. Bura, Y. Zhao, K. M. Burkin, K. Rafferty, C. T. Elliott, K. Campbell, *Sensors* **2019**, *19*, 5104.

[52] L. I. Labrecque, *Psychol. Mark.* **2020**, *37*, 855.

[53] K. Cantrell, M. M. Erenas, I. de Orbe-Payá, L. F. Capitán-Vallvey, *Anal. Chem.* **2010**, *82*, 531.

[54] G. Saravanan, G. Yamuna, S. Nandhini, in *Int. Conf. Commun. Signal Process.*, Melmaruvathur, India **2016**.

[55] F. Ricci, A. Vallée-Bélisle, K. W. Plaxco, *PLoS Comput. Biol.* **2011**, *7*, e1002171.

[56] Y. Rosenberg-Hasson, L. Hansmann, M. Liedtke, I. Herschmann, H. T. Maecker, *Immunol. Res.* **2014**, *58*, 224.

[57] W. S. Rasband, "ImageJ," can be found under https://imagej.nih.gov/ij/docs/faqs.html, **2018**.

[58] O. A. Akanbi, I. S. Amiri, E. Fazeldehkordi, in *A Machine-Learning Approach to Phishing Detection and Defence*, Syngress, Rockland, USA **2015**, p. 45.

[59] D. A. Armbruster, T. Pry, *Clin. Biochem. Rev.* **2008**, *29*, S49.